Engineered Single-Domain Antibodies with High Protease Resistance and Thermal Stability

Greg Hussack[1,2], Tomoko Hirama[1], Wen Ding[1], Roger MacKenzie[1,3], Jamshid Tanha[1,2,3]*

1 Institute for Biological Sciences, National Research Council Canada, Ottawa, Ontario, Canada, 2 Department of Biochemistry, Microbiology and Immunology, Faculty of Medicine, University of Ottawa, Ottawa, Ontario, Canada, 3 School of Environmental Sciences, University of Guelph, Guelph, Ontario, Canada

Abstract

The extreme pH and protease-rich environment of the upper gastrointestinal tract is a major obstacle facing orally-administered protein therapeutics, including antibodies. Through protein engineering, several *Clostridium difficile* toxin A-specific heavy chain antibody variable domains (V$_H$Hs) were expressed with an additional disulfide bond by introducing Ala/Gly54Cys and Ile78Cys mutations. Mutant antibodies were compared to their wild-type counterparts with respect to expression yield, non-aggregation status, affinity for toxin A, circular dichroism (CD) structural signatures, thermal stability, protease resistance, and toxin A-neutralizing capacity. The mutant V$_H$Hs were found to be well expressed, although with lower yields compared to wild-type counterparts, were non-aggregating monomers, retained low nM affinity for toxin A, albeit the majority showed somewhat reduced affinity compared to wild-type counterparts, and were capable of *in vitro* toxin A neutralization in cell-based assays. Far-UV and near-UV CD spectroscopy consistently showed shifts in peak intensity and selective peak minima for wild-type and mutant V$_H$H pairs; however, the overall CD profile remained very similar. A significant increase in the thermal unfolding midpoint temperature was observed for all mutants at both neutral and acidic pH. Digestion of the V$_H$Hs with the major gastrointestinal proteases, at biologically relevant concentrations, revealed a significant increase in pepsin resistance for all mutants and an increase in chymotrypsin resistance for the majority of mutants. Mutant V$_H$H trypsin resistance was similar to that of wild-type V$_H$Hs, although the trypsin resistance of one V$_H$H mutant was significantly reduced. Therefore, the introduction of a second disulfide bond in the hydrophobic core not only increases V$_H$H thermal stability at neutral pH, as previously shown, but also represents a generic strategy to increase V$_H$H stability at low pH and impart protease resistance, with only minor perturbations in target binding affinities. These are all desirable characteristics for the design of protein-based oral therapeutics.

Introduction

The gastrointestinal (GI) tract is the site of numerous microbial infections caused by a range of pathogens, including: *Helicobacter pylori*, *Salmonella* Typhi, *Vibrio cholerae*, *Escherichia coli*, *Campylobacter jejuni*, and *C. difficile*. The current approach for treating most of these infections involves administration of antibiotics, which places selection pressure on the organism, can lead to antibiotic resistance, and suppresses or eliminates beneficial commensal microbes. Disease-causing pathogens of the GI tract rely on a myriad of virulence factors for colonization, adherence, motility, cellular entry, and pathogenesis. These include, but are not limited to: surface-layer proteins, adhesins, invasins, flagella, high-molecular weight toxins, and quorum sensing molecules. Inhibition of bacterial virulence factors that are essential for disease pathogenesis therefore represents a novel, non-antibiotic based strategy to treat infectious diseases, while reducing the risk of microbial resistance and maintaining commensal gut populations [1,2,3].

Several approaches are being explored for antivirulence microbial therapy. Inhibition of *E. coli* pilus assembly [4], *Bacillus anthracis* lethal factor [5,6], Type III secretion systems [7,8],

Staphylococcus aureus quorum sensing pathways [9], cholera toxin [10] and *C. difficile* toxins A and B [11,12], with small molecules and peptides, are examples currently under development. One of the most pursued antivirulence strategies is targeting bacterial toxins with antibodies. Neutralizing antibodies against anthrax [13], shiga toxin [14], cholera toxin [15], botulinum toxin [16] and *C. difficile* toxins [17,18,19,20,21] have all been successfully isolated and a number of clinical trials involving antibodies to bacterial targets are underway [22]. For human pathogens that secrete toxins into the GI lumen before cellular entry, such as *C. difficile* [23], it may be advantageous to neutralize the toxins within the GI tract. Several studies indicate that oral administration of immunoglobulins (i.e., bovine Ig, human IgA, chicken IgY) may be successful at controlling various GI pathogens, including *C. difficile* [21,24], rotavirus [25], shigella [26], and enterotoxigenic *E. coli* in humans [27] and neonatal pigs [28]. However, there are major limitations facing orally administered immunotherapeutics, including the susceptibility of antibodies to proteolytic degradation, instability at low pH, high dosing requirements and cost [29].

Recombinant antibody fragments, such as single-domain antibodies (sdAbs) [30,31] isolated from conventional IgGs (i.e., V$_H$s, V$_L$s), from the heavy-chain IgG of *Camelidae* species (i.e.,

V$_H$Hs) and from cartilagous shark Ig$_{NARS}$ (i.e., V$_{NARS}$), are ideal agents to explore for oral immunotherapy [32] because of their small size (12 kDa–15 kDa), high affinity, high protease and thermal stability, high expression, amenability to library selection under denaturing conditions for isolating superstable species and ease of genetic manipulation. Despite possessing relatively high intrinsic protease and pH stability, a limited number of studies have shown that, when administered orally, sdAbs are readily degraded in the low pH pepsin-rich environment of the stomach and by digestive enzymes in the duodenum [33,34,35]. Several engineering and selection-based approaches have been undertaken to improve the thermal stability and protease resistance of sdAbs and other recombinant antibody fragments (i.e., scFvs and Fabs). Engineered disulfide bonds [36,37,38,39] and other stabilizing mutations [40] have increased the thermal stability of various recombinant fragments. Library selection of antibodies in the presence of proteases, denaturants, extreme pH, and elevated temperatures has lead to the isolation of antibody fragments with favorable characteristics such as improved thermal and chemical stability, increased protease resistance, and resistance to aggregation [41,42,43,44,45,46,47,48]. Random mutagenesis approaches have been used to increase the proteolytic stability of V$_H$Hs [49]. There has been no universal strategy to increase recombinant antibody thermal and protease stability simultaneously.

In this work, we hypothesized the addition of a non-canonical disulfide bond into the hydrophobic core of llama V$_H$Hs between framework region 2 (FR2) and FR3 would not only increase thermal stability at neutral pH, as previously reported [37,38,50], but would also impart resistance to proteolytic degradation and increase antibody stability at low pH. To test this hypothesis, we introduced two cysteine residues into a panel of V$_H$Hs which neutralize *C. difficile* toxin A (TcdA) [20]. Then, the mutant V$_H$Hs were compared to the wild-type V$_H$H counterparts with respect to expression yield, tendency for aggregation, antigen binding affinity, CD structural signatures, thermal stability at neutral and acidic pH, susceptibility to GI proteases, and toxin-neutralization capacity.

Methods

Chemicals, Reagents, and Cell Lines

All chemicals used in this study were of analytical grade supplied by various companies. Oligonucleotides were synthesized by Operon (Huntsville, AL). The vectors pSJF2H [51] or pMED2 (a modified version of pSJF2H containing *Sfi*I cloning sites) were used for all V$_H$H expression in *E. coli* cells (strain TG1) supplied by Stratagene (La Jolla, CA).

Cloning, Expression, and Purification of V$_H$H Mutants

The nomenclature used throughout this work to distinguish between wild-type and mutant V$_H$Hs is exemplified as follows: "A4.2" denotes a wild-type V$_H$H, "A4.2m" denotes a mutant V$_H$H. To construct mutant V$_H$Hs with a second disulfide bond, splice-overlap extension-polymerase chain reaction (SOE-PCR) [52] was performed using 4 primers for each V$_H$H (Table S1) and two rounds of PCR essentially as described [53]. Ala or Gly and Ile codons at positions 54 and 78 (IMGT numbering system; http://imgt.cines.fr/), respectively, were changed to Cys codons through primer-forced mutation. In the first PCR, two mutagenized overlapping sub-fragments were generated for each V$_H$H. The primer pairs used for each V$_H$H were as follows: A4.2m (BbsI-VHH and A4.2mR-Cys, A4.2mF-Cys and BamHI-VHH); A5.1m (BbsI-VHH and A5.1mRCys, A4.2mFCys and BamHI-VHH); A19.2m (BbsI-VHH and A19.2mR-Cys, A19.2mF-Cys and

BamHI-VHH); A20.1m (A20.1mSfiI-F and A20.1mR-Cys, A20.1mF-Cys and A20.1m*Sfi*I-R); A24.1m (A20.1mSfiI-F and A24.1mR-Cys, A24.1mF-Cys and A20.1mSfiI-R); A26.8m (BbsI-VHH and A26.8mR-Cys, A26.8mF-Cys and BamHI-VHH). Each sub-fragment was gel purified and spliced with its partner fragment in a second PCR. Briefly, 160 ng of each sub-fragment were added to a 50 μL PCR mixture containing *Pfu* DNA polymerase, dNTPs and reaction buffer. The reaction was placed in a thermal cycler and the two fragments were spliced together using a program consisting of a preheating step at 94°C for 5 min and 10 cycles of 94°C for 30 s, 55°C for 30 s, and 72°C for 1 min. To amplify the spliced products, the reaction was heated to 94°C for 3 min, 5 pmol (0.5 μL) of each primer pair was added (BbsI-VHH and BamHI-VHH for A4.2m, A5.1m, A19.2m, and A26.8m; A20.1mSfiI-F and A20.1mSfiI-R for A20.1m and A24.1m), and 35 PCR cycles were performed exactly as described above. The resulting fragments were gel purified, digested with *Bbs*I and *Bam*HI (A4.2m, A5.1m, A19.2m, and A26.8) or *Sfi*I (A20.1m and A24.1m) restriction enzymes, ligated into similarly digested expression vectors (pSJF2H or pMED2), and transformed into TG1 *E. coli* for V$_H$H expression. Positive colonies were identified by colony-PCR and DNA sequencing, using the M13RP and M13FP primers (Table S1).

Mutant V$_H$Hs were expressed in the same vector as wild-type V$_H$Hs [20]. Expression and purification of wild-type and mutant V$_H$Hs were performed as described [20], followed by dialysis into phosphate-buffered saline pH 7.3 (PBS), into distilled, deionized water (ddH$_2$O) for mass spectrometry (MS) analysis, or into 10 mM sodium phosphate buffer pH 7.3 for CD experiments.

MS Analysis

Proteolytic peptide fragments of mutant V$_H$Hs were created by digestion with cyanogen bromide (CNBr) and trypsin. Briefly, 100 μL reactions containing 50 μg of mutant V$_H$H (diluted in PBS), 10 μL of 1 M HCl and 40 μL of CNBr (10 mg/mL stock prepared in 1 M HCl) were digested for 14 h at ambient temperature in the dark. The next day, 100 μL of 1 M Tris-HCl, pH 8.6, and 60 μL of trypsin (100 μg/mL stock; sequencing grade, Roche, Mississauga, ON, Canada) were added directly to the CNBr reaction mixture and incubated for 2 h at 37°C. Samples were then analyzed by non-reducing SDS-PAGE to ensure digestion prior to MS analysis. Nano-flow reversed-phase HPLC MS (nanoRPLC-ESI-MS) with data dependent analysis (DDA) was performed to confirm disulfide bond formation in the mutant V$_H$Hs. An aliquot of the CNBr/trypsin digested V$_H$Hs was re-suspended in 0.1% formic acid (aq) and analyzed by nanoRPLC-ESI-MS using a nanoAcquity UPLC system coupled to a Q-TOF Ultima^{TM} hybrid quadrupole/TOF mass spectrometer (Waters). The peptides were first loaded onto a 180 μm I.D. ×20 mm 5 μm Symmetry®C18 trap (Waters), then eluted to a 100 μm I.D. ×10 cm 1.7 μm BEH130C18 column (Waters) using a linear gradient from 0% to 36% solvent B (acetonitrile + 0.1% formic acid) in 36 min, 36%–90% solvent B for 2 min. Solvent A was 0.1% formic acid in water. The peptide MS^2 spectra were searched against mutant V$_H$H protein sequences using the Mascot^{TM} database searching algorithm (Matrix Science, London, UK). The MS^2 spectra of the disulfide-linked peptides were deconvoluted using the MaxEnt 3 program (Waters) for *de novo* sequencing to determine the exact disulfide-linked positions.

Size Exclusion Chromatography and Affinity Measurements

Mutant V$_H$Hs were passed over a Superdex^{TM} 75 (GE Healthcare, Baie-d'Urfé, QC, Canada) size exclusion chromatog-

raphy column as described [20] to determine their aggregation state. Briefly, V_HHs were applied at concentrations ranging from 0.75–1 mg/mL ($\cong$45–60 μM) with a flow rate of 0.5 mL/min in a mobile phase that consisted of HBS-EP running buffer (10 mM HEPES, pH 7.4, 150 mM NaCl, 3 mM EDTA, and 0.005% (v/v) P20 surfactant). The collected fractions from the Superdex^{TM} 75 column were then used directly for surface plasmon resonance (SPR) analysis. All kinetic rate and equilibrium constants were determined as described [20] using a Biacore 3000 instrument (GE Healthcare) and 10,287 resonance units (RUs) of immobilized TcdA. In addition, the dissociation rate constants (k_{off}s) of mutant V_HHs before and after digestion with pepsin were compared by SPR (see below).

CD Spectroscopy

Wild-type and mutant V_HHs were analyzed by CD spectroscopy using a Jasco J-815 spectropolarimeter (Jasco, Easton, MD) at pH 7.3 (10 mM sodium phosphate buffer) and at pH 2.0 (10 mM sodium phosphate buffer+50 mM HCl). For all CD experiments performed at pH 2.0, proteins were equilibrated in the above buffer for a minimum of 2 h before scanning. The 50 mM Cl$^-$ concentration did contribute to a minor amount of light scatter at wavelengths less than 200 nm. For far-UV CD secondary structure scans and thermal unfolding experiments a 5 mm cuvette containing 1.5 mL of V_HH at 50 μg/mL (3.2 μM; $A_{280}\cong$0.1) was used. V_HH concentrations of up to 10 μM were initially tested, but signal intensities, expressed in molar ellipticity, were identical to that of 3.2 μM V_HH concentrations and this concentration also avoided generating compromising signals from protein aggregates formed at high temperatures in thermal unfolding experiments. In these experiments, 4 accumulations were collected for each sample between 190 nm–250 nm with a 1 mm bandwidth, 20 nm/min scan speed and 0.5 nm data pitch. Raw ellipticity data, given in millidegrees (mdeg), was smoothed using the Jasco software, exported, and converted to molar ellipticity, [θ]. To convert from mdeg to molar ellipticity ([θ]) in deg cm^2/dmol, Equation 1 [54] was used,

$$[\theta] = (m \deg \times MRW) \div (pathlength \times [V_H H]) \quad (1)$$

where the mean residue weight, MRW = (molecular weight of the antibody in Da/number of backbone amino acids), pathlength = cell pathlength in mm, and [V_HH] = concentration of V_HH in mg/mL. Thermal unfolding was followed at 215 nm with CD measurements taken every 2°C from 30°C to 96°C with a temperature increase of 1°C/min. It should be noted that 0.5°C and 1°C temperature interval measurements, on a select test V_HH, gave nearly identical T_m values to 2°C intervals. Molar ellipticity ([θ]) was used to calculate the fraction of protein folded (FF), which is shown in Equation 2 [55],

$$FF = ([\theta] - [\theta_U]) \div ([\theta_F] - [\theta_U]) \quad (2)$$

where [θ_F] and [θ_U] is the molar ellipticity of the folded (30°C) and unfolded (96°C) states, respectively. The thermal unfolding midpoint temperature (T_m) was obtained by plotting FF against temperature (T) and fitting with a sigmoidal Boltzmann function in GraphPad Prism (GraphPad Software, La Jolla, CA). We assumed a temperature of 30°C represented a fully folded V_HH (FF = 1.0) and a temperature of 96°C represented a fully unfolded V_HH (FF = 0). In the case of some V_HHs with a limited number of lower baseline data points, our T_m values are minimum estimates. We followed unfolding at 215 nm because of a large difference in ellipticity between folded and unfolded states at this wavelength and because of very low light scattering in samples measured at neutral and

acidic pH. A single T_m replicate for each V_HH was collected because of the very small standard error in CD-determined T_m values. For example, a number of previous V_HH T_m replicates in our lab, using identical conditions, produced a standard error ranging from ±0.03%–0.63% with an average error of ±0.33%.

To compare the tertiary structures of wild-type and mutant V_HHs at neutral and acidic pH, near-UV CD experiments were performed in the range of 250 nm–340 nm using the conditions described above with the exception of a 10 mm cuvette containing 2 mL of protein at 250 μg/mL. In all cases, the ellipticity of buffer blanks were subtracted from experimental values and the reported data is the average of two independent experiments with 4 data accumulations in each.

Protease Digestion Assays

The sensitivity of wild-type and mutant V_HHs to the three major GI proteases pepsin, trypsin, and chymotrypsin was explored. All reactions were performed in 20 μL volumes with 4.8 μg of V_HH diluted in PBS. For pepsin digestions, reactions contained 17 μL of V_HH, 2 μL of porcine stomach pepsin (460 U/mg; Sigma, Mississauga, ON, Canada), and 1 μL of 1 M HCl (final pH: 2.0). Final pepsin concentrations in each reaction ranged from 0.1 μg/mL to 100 μg/mL. Digestions were incubated at 37°C for 1 h and neutralized with 1 μL of 1 M NaOH. For trypsin and chymotrypsin digestions, reactions contained 18 μL of V_HH (diluted in PBS supplemented with 10 mM CaCl$_2$) and 2 μL of either trypsin or chymotrypsin (sequencing grade, Roche). Final trypsin/chymotrypsin concentrations ranged from 0.1 μg/mL to 100 μg/mL. Digestions were incubated at 37°C for 1 h and neutralized with 1 μL of protease inhibitor cocktail (Sigma). All neutralized V_HH-protease reactions and controls (V_HHs with no protease) were separated by SDS-PAGE, stained with Coomassie and photographed using an AlphaImager3400 (Alpha Innotech Corporation, San Leandro, CA). To determine the percent of V_HH retained after protease digestions, densitometry analysis was performed using the AlphaEaseFc software package (Version 7.0.1, Alpha Innotech Corporation) on control and digested V_HHs. A total of three independent digestion reactions were performed on all of the V_HHs at each protease concentration and replicate digestions were run on separate SDS-PAGE gels. Digestions at the highest protease concentration (100 μg/mL) that were not analyzed by SDS-PAGE were buffer exchanged into ddH$_2$O using Millipore Biomax 5K MWCO spin columns (Millipore, Billerica, MA) and subjected to MS analysis to identify the cleavage products, or analyzed by SPR for TcdA binding activity.

Toxin Neutralization Assay

In vitro TcdA neutralization assays were performed essentially as described [20]. Human lung fibroblast cell rounding was reported 24 h post addition of TcdA (100 ng/mL), TcdA+wild-type V_HH (1000 nM) or TcdA+mutant V_HH (1000 nM). Specifically, V_HHs were added as pooled mixtures of A4.2, A5.1, A20.1, and A26.8 (250 nM each, 1000 nM total) or A4.2m, A5.1m, A20.1m, and A26.8m (250 nM each, 1000 nM total). The percentage of cell rounding was scored visually using light microscopy and the reported values are the average of two independent experiments in which each V_HH mixture was tested in triplicate.

Homology Modeling

The SWISS-MODEL online workspace (http://swissmodel. expasy.org/workspace/) [56] was used to construct homology models of A4.2 (wild-type) and A4.2m (mutant) V_HHs. The 1qd0A (PDB) V_HH was used as a template [57], sharing 73.5% and
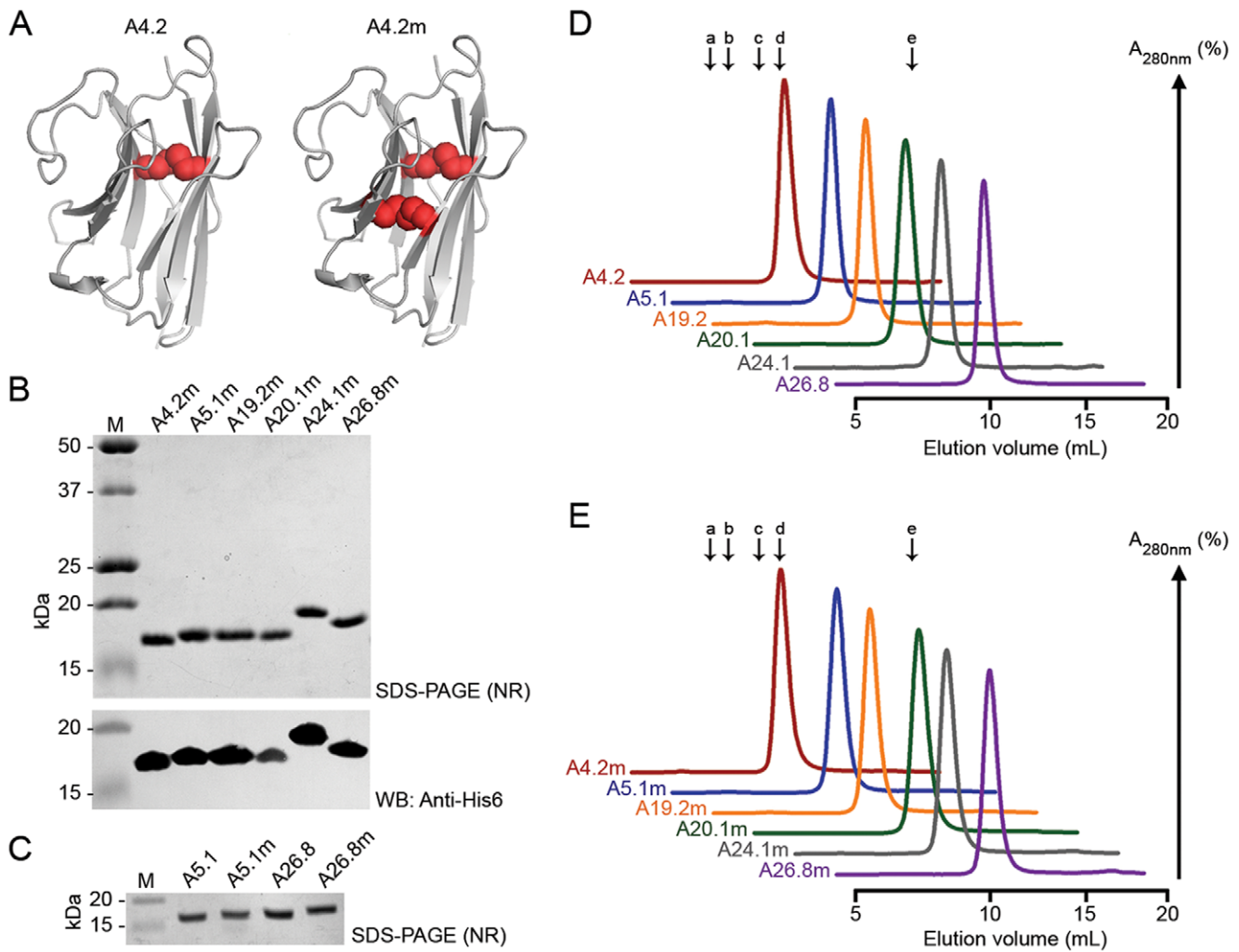
Figure 1. Design, purification, and size exclusion chromatography profiles of disulfide bond mutant V$_H$Hs. (**A**) Representative homology models of A4.2 and A4.2m were built on the PDB template 1qd0A V$_H$H [57], sharing 73.5% and 71.8% homology, respectively. Disulfide bonds are shown as colored spheres in the hydrophobic core of the V$_H$H domains. (**B**) Non-reducing (NR) SDS-PAGE analysis and Western blot (WB) probed with an anti-His$_6$ IgG on IMAC-purified mutant V$_H$Hs. M: molecular weight marker in kDa. (**C**) Representative SDS-PAGE analysis showing mutant V$_H$Hs run slower than the corresponding wild-type V$_H$Hs under non-reducing conditions. (**D, E**) Size exclusion chromatography (SEC) analysis of wild-type and mutant V$_H$Hs revealed similar size exclusion profiles, indicating the second disulfide bond does not promote the formation of interdomain disulfide-bonds or multimeric mutant V$_H$Hs. The elution volumes (V$_e$s) of SEC molecular weight standards are shown with arrows and are aligned relative to the A4.2 and A4.2m chromatograms. a: ovalbumin (MW = 43.0 kDa, V$_e$ = 8.90 mL); b: carbonic anhydrase (MW = 30.0 kDa, V$_e$ = 9.71 mL); c: trypsin inhibitor (MW = 20.1 kDa, V$_e$ = 11.06 mL); d: α-lactalbumin (MW = 14.4 kDa, V$_e$ = 11.97 mL); e: vitamin B (MW = 1.3 kDa, V$_e$ = 18.7 mL). The equation of the line of a standard curve generated from these standards was $LOG_{10}MW = -0.1539 V_e + 2.9949$ ($r^2 = 0.9995$). From this equation the V$_H$H apparent MWs ranged from 9.8 kDa–13.6 kDa, indicating monomeric V$_H$Hs.
doi:10.1371/journal.pone.0028218.g001

71.8% homology, respectively. Images of the modeled V$_H$Hs were generated using PyMOL (www.pymol.org).

Results

Expression and Purification of Mutant V$_H$Hs

Previously, a unique dromedary "V$_H$H" was isolated that possessed a naturally occurring disulfide bond between Cys54 and Cys78 residues [58]. When incorporated into several "wild-type" V$_H$Hs which possessed only the conserved Cys23/Cys104 disulfide bond, the Cys54/Cys78 disulfide bond increased V$_H$H thermal and chemical stabilities [37,38]. To examine the stabilizing effects of an engineered disulfide bond on llama-derived V$_H$Hs, we followed this strategy and chose to introduce two cysteine residues into the hydrophobic core of six *C. difficile* TcdA-specific V$_H$Hs

[20] by incorporating Ala/Gly54Cys and Ile78Cys point mutations (Fig. 1A, Fig. S1), creating V$_H$Hs with two disulfide bonds. Soluble V$_H$Hs were extracted from the periplasm of TG1 *E. coli* and purified by immobilized-metal affinity chromatography (IMAC) with purified yields ranging from 3–12 mg/L of bacterial culture. Non-reducing SDS-PAGE and Western blot analysis of the purified products revealed the mutant V$_H$Hs were of high purity and did not form interdomain disulfide bonds (Fig. 1B). On non-reducing SDS-PAGE gels, mutant V$_H$Hs consistently ran slower than their corresponding wild-type V$_H$Hs (Fig. 1C).

MS Analysis

The molecular weights of all mutant V$_H$Hs were determined, but were not accurate enough to confirm the formation of the engineered disulfide bond. To precisely confirm the presence of

the introduced disulfide bond, mutant V_HHs were digested with CNBr and trypsin (Fig. 2A, B) and their digests subjected to MS^2 analysis. The identification coverage of the mutant V_HHs from the analysis of their CNBr/trypsin digests using nanoRPLC-ESI-MS with DDA was more than 30%. The disulfide-linked peptide ions appeared prominent in the survey scan of the DDA experiment when the proteins were digested with a combination of CNBr and trypsin. Peptide fragments linked by the engineered Cys^{54}–Cys^{78} disulfide bond (shown in blue text in Fig. S1) were positively identified for all mutant V_HHs by manual de-novo sequencing (Table 1). For example, the protein sequence coverage of A5.1m was 43% and a prominent ion at m/z 526.25 (3+) was sequenced as a disulfide-linked peptide EFVCVITR (P1) and FTCSR (P2) as shown (Fig. 2C, Fig. S1, Table 1). An almost complete disulfide-linked y fragment ion series was observed from one peptide with the other peptide attached as a modification via a disulfide bond, which remains intact under collision induced dissociation (CID) [59].

Size Exclusion Chromatography and Affinity Measurements

Analysis of mutant V_HHs on a Superdex™ 75 size exclusion chromatography column produced single, monomeric peaks nearly identical to the profile for wild-type V_HHs (Fig. 1D, E), confirming the mutant V_HHs are non-aggregating. SPR analysis revealed the specific and high-affinity binding of 4 of 6 mutant V_HHs to TcdA (Fig. 3, Table 2). These four were also the strongest TcdA neutralizers. Two mutants (A19.2m and A24.1m) exhibited non-specific binding to reference cell proteins and as a result specific interaction data could not be generated, even at antibody concentrations as high as 3.2 μM. When compared to their wild-type counterparts, the K_{DS} of 3 TcdA-binding mutants were reduced approximately 2–6 fold (Table 2), while the affinity of one V_HH was relatively unchanged (K_{DS} of 24 nM and 20 nM for A4.2 and A4.2m, respectively). The K_D reductions were largely a result of faster k_{off} values and to a much lesser extent influenced by
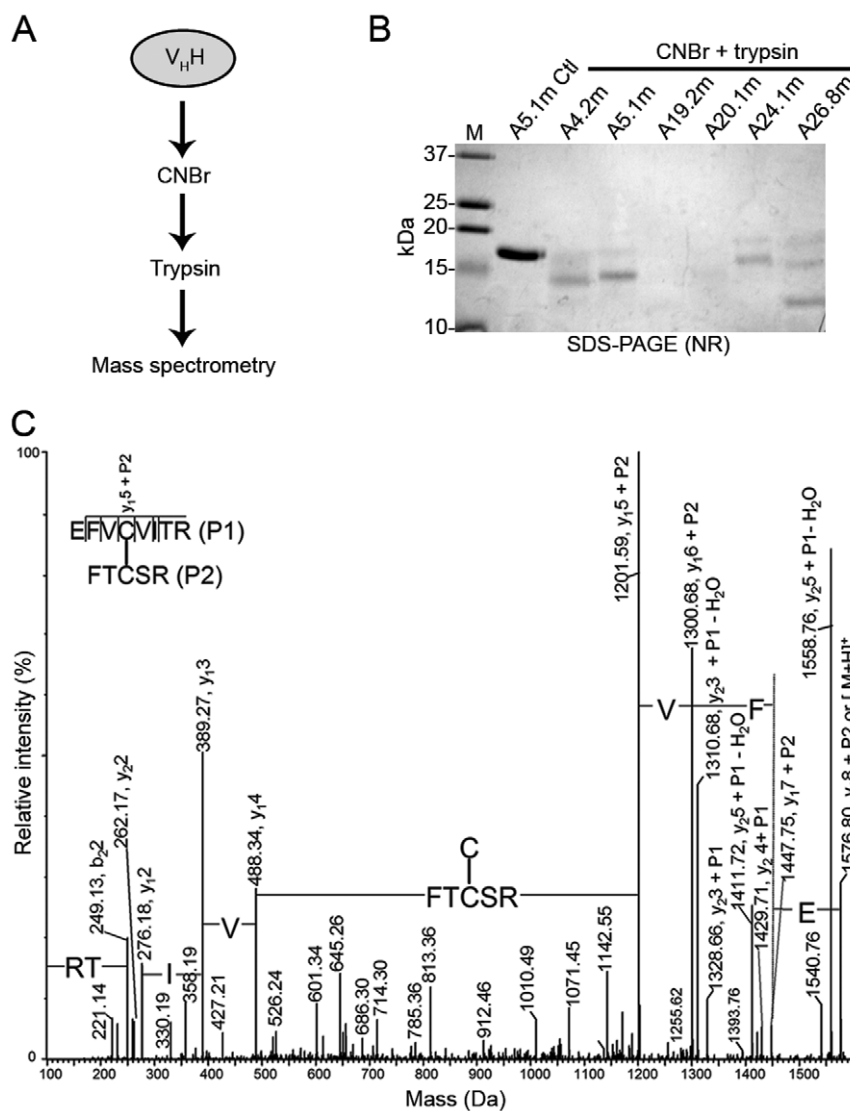

Figure 2. Disulfide bond formation between residues Cys[54] and Cys[78] is confirmed by MS². (**A**) Schematic diagram of mutant V_HH digestion with cyanogen bromide (CNBr) and trypsin before MS^2 analysis. (**B**) V_HHs (3 μg per lane) were subjected to SDS-PAGE analysis under non-reducing (NR) conditions to illustrate near complete digestion with CNBr and trypsin. Untreated A5.1m was added as a control (Ctl). M: molecular weight marker in kDa. (**C**) MaxEnt 3 deconvoluted CID-MS^2 spectrum of the m/z 526.25 (3+) ion of the disulfide-linked peptide EFVCVITR (P1) – FTCSR (P2), encompassing the Cys[54]–Cys[78] disulfide bond, from CNBr/trypsin digested A5.1m.
doi:10.1371/journal.pone.0028218.g002

Table 1. Disulfide linkage determination of mutant V_HHs by MS^2 analysis.

V_HH	CNBr/tryptic peptides	MW_{for}	MW_{exp}	ΔMW
A4.2m	EFV**C**AVSR FT**C**SR	1519.69	1519.70	−0.01
A5.1m	EFV**C**VITR FT**C**SR	1575.75	1575.76	−0.01
A19.2m	EFV**C**GISR FT**C**SR	1519.69	1519.64	0.05
A20.1m	EFV**C**AGSSTGR FT**C**SR	1722.74	1722.84	−0.10
A24.1m	EFV**C**GISWGGGSTR FT**C**SR	2064.91	2064.98	−0.07
A26.8m	EFV**C**VISSTGTSTYYADSVK FT**C**SR	2766.25	2766.33	−0.08

Mutant V_HHs were digested with CNBr and trypsin and the peptides analyzed by MS^2. The peptides containing the Cys^{54}–Cys^{78} disulfide linkage are shown with connecting cysteines bolded. A nearly perfect match between MW_{for} and MW_{exp} equates to the presence of the Cys^{54}–Cys^{78} disulfide linkage. MW_{for}: formula (expected) molecular weight (Da); MW_{exp}: experimental molecular weight (Da); $\Delta MW = MW_{for} - MW_{exp}$.
doi:10.1371/journal.pone.0028218.t001

slower k_{on} values. In general, these data suggest the Cys^{54}–Cys^{78} disulfide bond may slightly distort the V_HH structure leading to decreases in target binding affinities and decreases in antibody specificity.

V_HH Structural and Thermal Stability Characterization

CD experiments were used to examine V_HH secondary structure, tertiary structure, and thermal stability at both neutral and acidic pH. We first examined V_HH secondary structure by far-UV CD (Fig. 4A, Fig. S2). Although the overall shape of the far-UV CD spectra from wild-type and mutant V_HH pairs was similar at a given pH, spectra intensity shifts were observed for all wild-type/mutant pairs. In general, peak minima were seen at 216 nm–218 nm and at 230 nm–235 nm wavelengths but, in almost all cases, the intensity of the peak at 216 nm–218 nm was lower (decreased negative ellipticity) for mutant V_HHs. Another prominent feature in the far-UV CD spectra was that mutant V_HHs exhibited a near-UV shift in the peak range of 230 nm–235 nm. Wild-type V_HHs possessed peak minima around 230 nm–232 nm whereas mutants displayed peak minima in this region around 232 nm–235 nm. Interestingly, A4.2/A4.2m, which of all the wild-type/mutant pairs had the most similar CD spectra at neutral pH, also had the same binding affinity for TcdA.

We next examined V_HH tertiary structures with near-UV CD spectroscopy (Fig. 4B, Fig. S3). The CD spectra in this region (250 nm–320 nm) come primarily from aromatic residues within the V_HH, with Phe contributing in the range of 250 nm–270 nm, Tyr contributing in the range of 270 nm–290 nm, and Trp contributing in the range of 280 nm–300 nm. Overall, the near-UV spectra profiles were similar between wild-type and mutant V_HH pairs. Spectra from wild-type and mutant pairs shared nearly identical peak wavelengths; however, between 250 nm to 295 nm, the ellipticity of mutant V_HHs was consistently more negative than wild-type V_HHs. There were also subtle differences in peaks occurring around 297 nm, with mutant V_HHs exhibiting a minor but consistent shift to the right. Three of the four wild-type/mutant pairs (A4.2/A4.2m, A5.1/A5.1m, and A20.1m/A20.1m) produced predominantly negative ellipticity, whereas the A26.8/A26.8m pair remained positive. The contributions of the second disulfide bond cannot be ruled out as a factor which may augment the contribution of aromatic residues to ellipticity (increasing negatively) of the mutants.

Finally, temperature-induced unfolding experiments were conducted in order to determine V_HH T_ms and $T_{onset}s$ by following changes in V_HH ellipticity at 215 nm (Fig. 5, Fig. S4, Table 3, Table S2). All V_HHs exhibited sigmoidal melting curves, indicative of cooperative unfolding of a protein that exists in either a folded or unfolded state. The wild-type V_HHs already have high T_ms (as high as 84.7°C) – significantly higher than those reported for other V_HHs [60]. At neutral pH, all mutant V_HHs had significantly higher thermal unfolding midpoint temperatures (p = 0.031, unpaired two-tailed t-test) than their wild-type V_HH counterparts. The T_m values of mutants ranged from 78.8°C to 93.6°C, with one mutant, A5.1m, having a T_m 11.6°C higher than wild-type (A5.1). The increase in mutant V_HH T_ms relative to wild-type ranged from 3.7°C to 11.6°C. Overall, at neutral pH, the mean T_m ± SEM was 76.2°C±1.8°C and 83.6°C±2.3°C for wild-type and mutant V_HHs, respectively (Fig. 5B). These findings are in agreement with previous reports that showed significant increases in the T_ms of disulfide bond engineered V_HHs [37,38,50]. In a second series of experiments, temperature-induced unfolding was conducted at pH 2.0 by once again following V_HH ellipticity changes at 215 nm (Fig. 5, Fig. S4, Table 3). At acidic pH a considerable reduction in T_m was observed for both wild-type (22.1°C to 32.4°C) and mutant V_HHs (23.7°C to 31.2°C) when compared to the T_m values recorded at pH 7.3. However, at acidic pH the T_m of all six mutants was still significantly higher than the corresponding wild-type V_HHs (p = 0.002, unpaired two-tailed t-test). In acid, the increase in mutant V_HH T_ms relative to wild-type ranged from 2.1°C to 11.6°C, which is a nearly identical spread in temperature increases to that seen at neutral pH. Overall, at pH 2.0, the mean T_m ± SEM was 49.3°C±1.2°C and 56.6°C±1.2°C for wild-type and mutant V_HHs, respectively (Fig. 5B). Interestingly, the highest T_m gains at both pHs were seen for the four strongest neutralizers. The T_m differences between wild-type/mutant pairs are more significant at acidic pH than neutral pH. Taken together, these results (Table 3; Fig. 5) suggest the Cys^{54}–Cys^{78} disulfide bond may stabilize the V_HHs from acid-induced denaturation. Using our thermal unfolding curves, we also identified V_HH T_{onset} temperatures, the temperature at which 5% of the V_HH was unfolded (Fig. 5C; Table S2). The T_{onset} of mutant V_HHs was significantly higher than wild-type V_HHs at both neutral and acidic pH (p = 0.027 and p = 0.006, respectively, unpaired two-tailed t-test). The T_{onset} differences between wild-type/mutant pairs are more significant at acidic pH than neutral pH. At pH 7.3, the mean T_{onset} ± SEM was 68.9°C±1.8°C and 74.9°C±1.5°C for wild-type and mutant V_HHs, respectively. At pH 2.0, the mean T_{onset} ± SEM was 41.2°C±1.3°C and 47.3°C±1.3°C for wild-type and mutant V_HHs, respectively. Therefore, the lowest T_{onset} for the mutants was 45.0°C, whereas two of the wild-type V_HHs (A5.1, A20.1) already had $T_{onset}s$ of ~37°C at pH 2.0 (physiological stomach conditions).

Protease Digestion Assays

Proteins traveling through the GI tract encounter low pH and digestive enzymes in the stomach. We therefore asked if the Cys^{54}–Cys^{78} disulfide bond improved V_HH resistance to proteolytic degradation. We compared the effects of the major GI proteases pepsin, trypsin, and chymotrypsin on wild-type and mutant V_HHs through SDS-PAGE and MS analysis. Initially, protease concentrations of 0.1 µg/mL, 1 µg/mL, 10 µg/mL, and 100 µg/mL were explored. When the lowest concentrations of proteases (0.1 µg/mL and 1 µg/mL) were used in digestion reactions, wild-type and mutants appeared similar to undigested controls on SDS-PAGE (data not shown). Similarly, V_HHs were only moderately
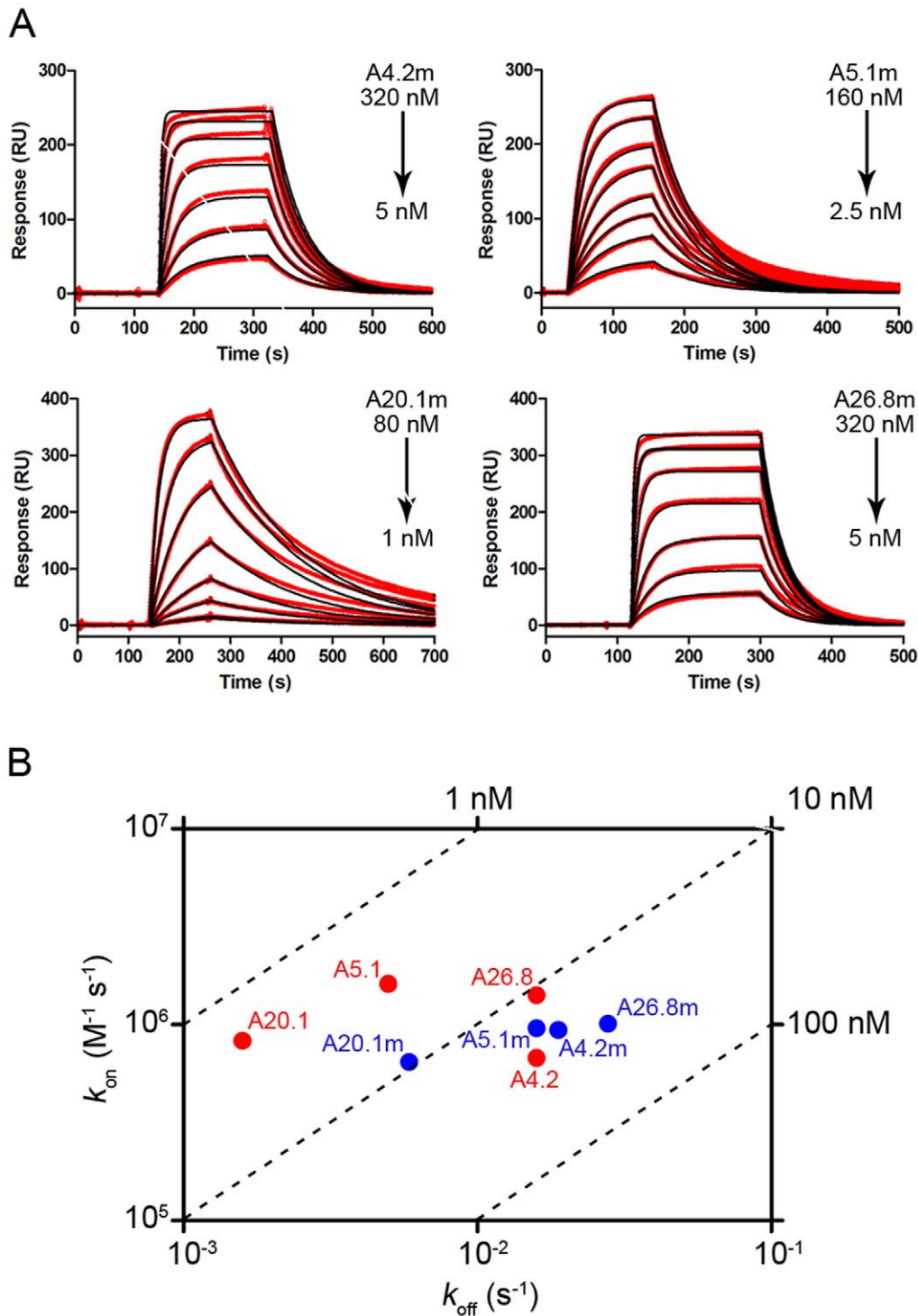
Figure 3. Mutant V$_H$Hs retain high affinity binding to TcdA. (**A**) SPR sensorgrams demonstrating mutant V$_H$Hs retained high affinity binding to immobilized *C. difficile* TcdA. The range of V$_H$H concentrations used in each experiment is shown. Red lines represent measured interaction data, and black lines represent fitted curves. The kinetic and affinity constants are reported in Table 2. Binding of A19.2m and A24.1m to TcdA was non-specific, and the kinetic and affinity constants could not be determined. (**B**) Rate plane plot with iso-affinity diagonals comparing wild-type (red) and mutant V$_H$Hs (blue).
doi:10.1371/journal.pone.0028218.g003

susceptible to protease degradation at 10 µg/mL (data not shown). In order to see clear differences in the proteolytic susceptibility of wild-type and mutant V$_H$Hs, all remaining digestions were performed at protease concentrations of 100 µg/mL. SDS-PAGE

analysis of pepsin-digested wild-type and mutant V$_H$Hs showed a reduction in V$_H$H size from ~16 kDa (control) to either ~14 kDa, or complete digestion to smaller fragments (Fig. 6A). The band at ~14 kDa routinely appeared in digestions with each of the

Table 2. Kinetic and affinity constants of wild-type and mutant V_HHs.

V_HH	Wild-type[a]			Mutant			Fold change in K_D[b]
	k_{on} (M^{-1} s^{-1})	k_{off} (s^{-1})	K_D (nM)	k_{on} (M^{-1} s^{-1})	k_{off} (s^{-1})	K_D (nM)	
A4.2/A4.2m	6.7×10^5	1.6×10^{-2}	24	9.3×10^5	1.9×10^{-2}	20	−1.2
A5.1/A5.1m	1.6×10^6	5.0×10^{-3}	3	9.5×10^5	1.6×10^{-2}	17	+5.7
A19.2/A19.2m	1.4×10^4	3.9×10^{-3}	290	–	–	–	
A20.1/A20.1m	8.2×10^5	1.6×10^{-3}	2	6.4×10^5	5.9×10^{-3}	9.2	+4.6
A24.1/A24.1m	6.0×10^4	1.6×10^{-2}	260	–	–	–	
A26.8/A26.8m	1.4×10^6	1.6×10^{-2}	12	1.0×10^6	2.8×10^{-2}	28	+2.3

[a]Data obtained from [20].
[b]Relative to wild-type V_HH.
doi:10.1371/journal.pone.0028218.t002

proteases. Similar to V_H protease digestion studies [61], MS mass analysis on the ~14 kDa products revealed cleavage at various positions within the V_HH C-terminal c-Myc epitope tag. Loss of the epitope tag corresponded to reductions of 1641.7 Da, 1754.8 Da, and 1641.7 Da for pepsin, trypsin, and chymotrypsin digested V_HHs, respectively (data not shown).

Overall, significant increases in pepsin resistance were found for all mutant V_HHs compared to their wild-type counterparts (p = 0.026, Mann-Whitney U test) (Fig. 6B; Fig. 7; Table 4). The increase in mutant V_HH pepsin resistance relative to corresponding wild-type ranged from almost 4.5% to 63% (Table 4). For example, A5.1 was completely degraded after incubation with pepsin, while nearly 50% of A5.1m remained intact (Fig. 6A, B). The biggest increase in pepsin resistance was found for A4.2m, where an almost 63% increase in intact V_HH structure was found

relative to A4.2. Interestingly, A4.2m also had the highest T_m and T_{onset} at pH 2.0 (Table 3; Table S2), the same pH at which the pepsin digestions were performed. Increases in mutant V_HH resistance to chymotrypsin were not as universal (Fig. 7; Fig. S5, Table 4) but, nonetheless, 4 of 6 mutant V_HHs showed increased resistance to chymotrypsin, with significant increases found in clones A5.1m, A24.1m, and A26.8m (p<0.05) compared to their wild-type counterparts. No statistical differences were found between trypsin digested wild-type and mutant V_HHs (Fig. 7; Fig. S5, Table 4), except for A4.2m, where trypsin resistance was actually reduced from almost 36% in the wild-type V_HH to almost 5% in the mutant. Both the wild-type and mutant versions of A19.2 and A26.8 were very susceptible to trypsin degradation.

A correlation was observed between V_HH pepsin resistance and T_ms at pH 2.0 (r^2 = 0.735, Fig. 8A). The wild-type V_HHs with
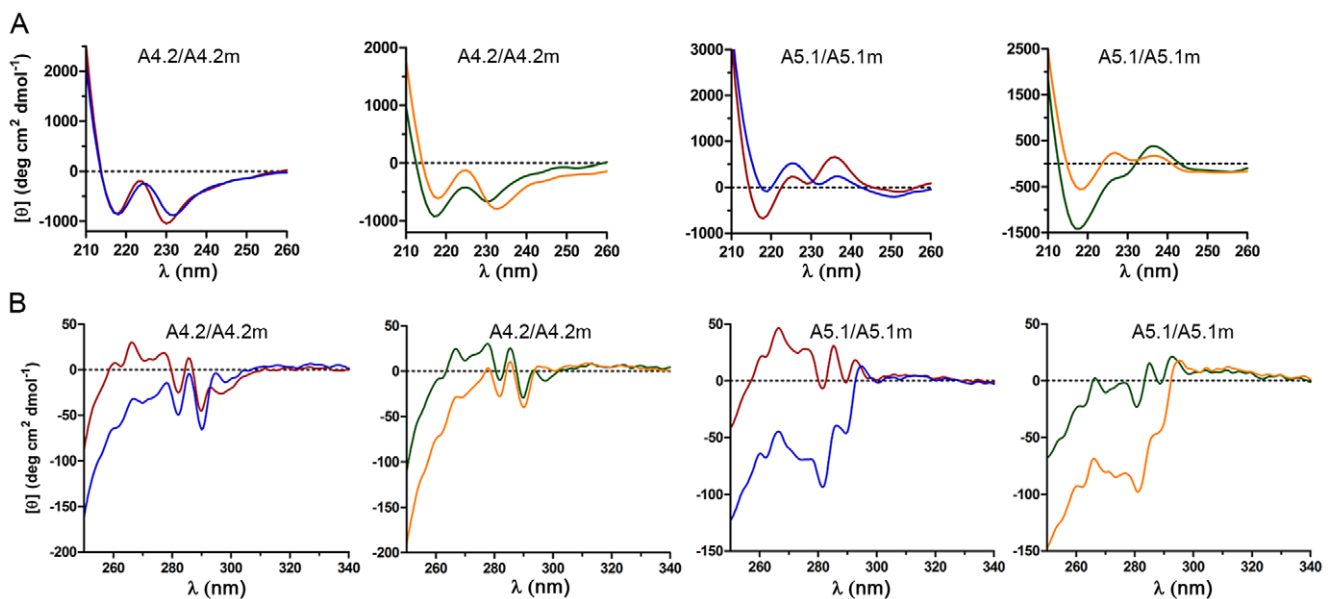

Figure 4. Representative far-UV and near-UV CD spectra of wild-type and mutant V_HHs at neutral and acidic pH. Far-UV CD spectra (**A**) and near-UV CD spectra (**B**) of A4.2/A4.2m and A5.1/A5.1m at neutral and acidic pH. Far-UV scans (210 nm–260 nm) were performed at 25°C on V_HHs (50 µg/mL) equilibrated for 2 h in 10 mM sodium phosphate buffer (pH 7.3) or 10 mM sodium phosphate buffer+50 mM HCl (pH 2.0) in a 5 mm cuvette. Near-UV scans (250 nm–340 nm) were performed at 25°C on V_HHs (250 µg/mL) under similar conditions in a 10 mm cuvette. All spectra represent the mean residue ellipticity from 8 data accumulations collected from 2 independent experiments. Raw data were smoothed using the Jasco software and converted to mean residue ellipticity as described in *Methods*. Red lines: wild-type V_HH at pH 7.3; blue lines: mutant V_HH at pH 7.3; green lines: wild-type V_HH at pH 2.0; orange lines: mutant V_HH at pH 2.0.
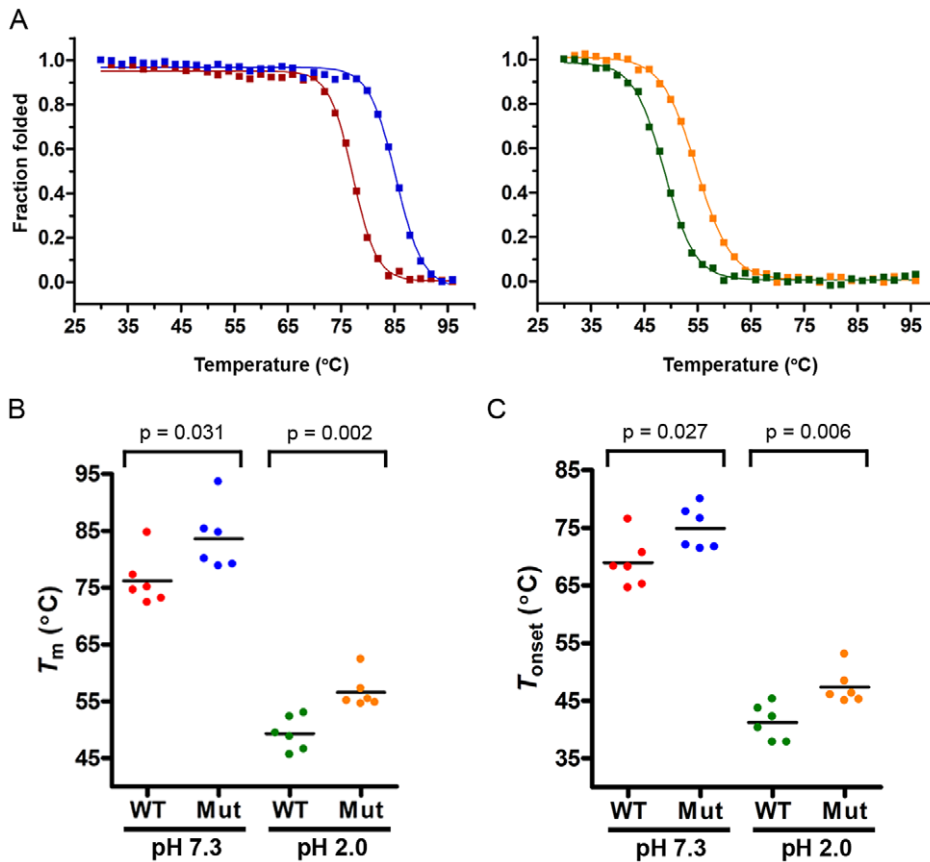doi:10.1371/journal.pone.0028218.g004

Figure 5. Mutant V$_H$H thermal unfolding midpoint temperatures are significantly greater than those of wild-type V$_H$Hs. (**A**) Representative example showing the thermal unfolding of A26.8 (WT) and A26.8m (Mut) at neutral pH (*left*) and acidic pH (*right*). V$_H$H thermal unfolding midpoint temperatures (T_ms) were determined using CD spectroscopy by following antibody unfolding (50 µg/mL) at 215 nm in 10 mM sodium phosphate buffer +/−50 mM HCl. Raw data were converted to fraction folded, as described in *Methods*, and the T_m was determined by Boltzmann sigmoidal curve fitting (r^2 ranging from 0.9965–0.9995). T_{onset} was determined from the same curve and was defined as the temperature at which 5% of the V$_H$H was unfolded. Red lines: wild-type V$_H$H at pH 7.3; blue lines: mutant V$_H$H at pH 7.3; green lines: wild-type V$_H$H at pH 2.0; orange lines: mutant V$_H$H at pH 2.0. (**B**) Summary of V$_H$H T_ms. (**C**) Summary of V$_H$H T_{onset}s. In *B* and *C*, dots represent individual V$_H$Hs and the black bars represent the mean T_m or T_{onset}, respectively. P-values were determined using the unpaired two-tailed *t*-test.
doi:10.1371/journal.pone.0028218.g005

lower T_ms occupied the low protease resistance region of the graph, the mutants with higher T_ms occupied the high protease resistance region of the graph. There was also a moderate correlation between V$_H$H pepsin resistance and T_ms at pH 7.3 (r^2 = 0.500, data not shown). No correlation was evident between

Table 3. Thermal unfolding midpoint temperatures (T_m) of wild-type and mutant V$_H$Hs.

V$_H$H	T_m (°C) at pH 7.3			T_m (°C) at pH 2.0		
	Wild-type	Mutant	ΔT_m	Wild-type	Mutant	ΔT_m
A4.2/A4.2m	84.7*	93.6*	8.9	52.3	62.4	10.1
A5.1/A5.1m	73.1	84.7*	11.6	45.6	57.2	11.6
A19.2/A19.2m	75.1	78.8	3.7	53.0	55.1	2.1
A20.1/A20.1m	72.4	79.1	6.7	46.6	55.4	8.8
A24.1/A24.1m	74.6	80.1	5.5	49.4	54.6	5.2
A26.8/A26.8m	77.2	85.3*	8.1	48.8	54.8	6.0

*Minimum estimated T_m.
doi:10.1371/journal.pone.0028218.t003

V$_H$H trypsin resistance and T_ms at pH 7.3 or pH 2.0 (r^2 = 0.138 and r^2 = 0.138, respectively) or between V$_H$H chymotrypsin resistance and T_ms at pH 7.3 or pH 2.0 (r^2 = 0.012 and r^2 = 0.004, respectively). In addition, a strong correlation between wild-type V$_H$H pepsin resistance and wild-type V$_H$H T_{onset} at pH 2.0 was noted (r^2 = 0.975, Fig. 8B, Table S2). No correlation was evident between mutant V$_H$H pepsin resistance and mutant V$_H$H T_{onset} at pH 2.0 (r^2 = 0.191), presumably because mutant V$_H$H T_{onset} temperatures were much higher than the temperature at which pepsin digestions were performed (37°C). Interestingly, we also noted a correlation between V$_H$H trypsin resistance and the theoretical number of trypsin cleavage sites located within the whole V$_H$H (r^2 = 0.822) or located within the V$_H$H CDR (r^2 = 0.681) regions (Table S3, Fig. S6). No correlation was found between V$_H$H pepsin or chymotrypsin resistance and the theoretical number of pepsin or chymotrypsin cleavage sites, respectively (Fig. S6).

The ability of pepsin-treated mutants (A4.2m, A5.1m, A20.1m, and A26.8m) to bind TcdA was evaluated by SPR. SPR analyses confirmed the mutants ("V$_H$H−tag"; *see* Fig. 6A) retained TcdA binding as their k_{off} values were essentially the same as those of untreated controls (Table 2; Fig. 6C). SPR analysis on pepsin-digested wild-type V$_H$Hs could not be performed since these

Figure 7. Summary of V_HH resistance profiles to pepsin, trypsin, and chymotrypsin. V_HH resistance to the major GI proteases was determined by proteolytic digestion (100 μg/mL protease, 37°C, 1 h) and SDS-PAGE densitometry analysis. Dots represent the mean (n = 3) protease resistance profile of each V_HH relative to undigested controls and the black bars represent the median resistance of each group. P-values were determined using the unpaired two-tailed Mann-Whitney U test. WT: wild-type V_HH; Mut: mutant V_HH; Chymo: chymotrypsin.
doi:10.1371/journal.pone.0028218.g007

Toxin Neutralization Assay

Mutant V_HHs retained their ability to neutralize to cytotoxic effects of TcdA on monolayers of fibroblast cells. Comparison of the neutralization capacity of pooled mixtures (1000 nM total) of wild-type and mutant V_HHs revealed mutants performed nearly as well as wild-types at reducing TcdA-mediated cell rounding (Fig. 9). Given that 3 of 4 mutants showed weaker affinity for TcdA the reduction in neutralizing capacity relative to wild-type V_HHs was not unexpected.

Discussion

The rapid development of bacterial resistance to most major classes of antibiotics has created a demand for novel therapeutics in the fight against infectious diseases. One of the most pursued non-antibiotic strategies involves targeting bacterial virulence factors with small molecules and antibodies. For some pathogens, inhibition of toxins and colonization factors within the GI tract may be an effective means of disease control. Oral immunotherapy for treating infectious diseases has had limited success due to the instability of immunoglobulins in the extreme pH and protease-rich environment of the GI tract. Here, through protein engineering, we increased the protease, acid and thermal stability of llama-derived sdAbs (V_HHs) which target and neutralize *C. difficile* toxin A without dramatically affecting biological function.

Our stabilization strategy involved the substitutions of two amino acid residues at positions 54 and 78 for cysteine, allowing for the formation of a second, non-native disulfide bond between FR2 and FR3 in the V_HH hydrophobic core. Incorporation of a disulfide bond at these positions has been previously reported in camelid V_HHs [37,38,50] and was found to increase V_HH chemical and thermal stability. We hypothesized that the additional disulfide bond may also enhance V_HH resistance to proteases, especially in denaturing acidic conditions.
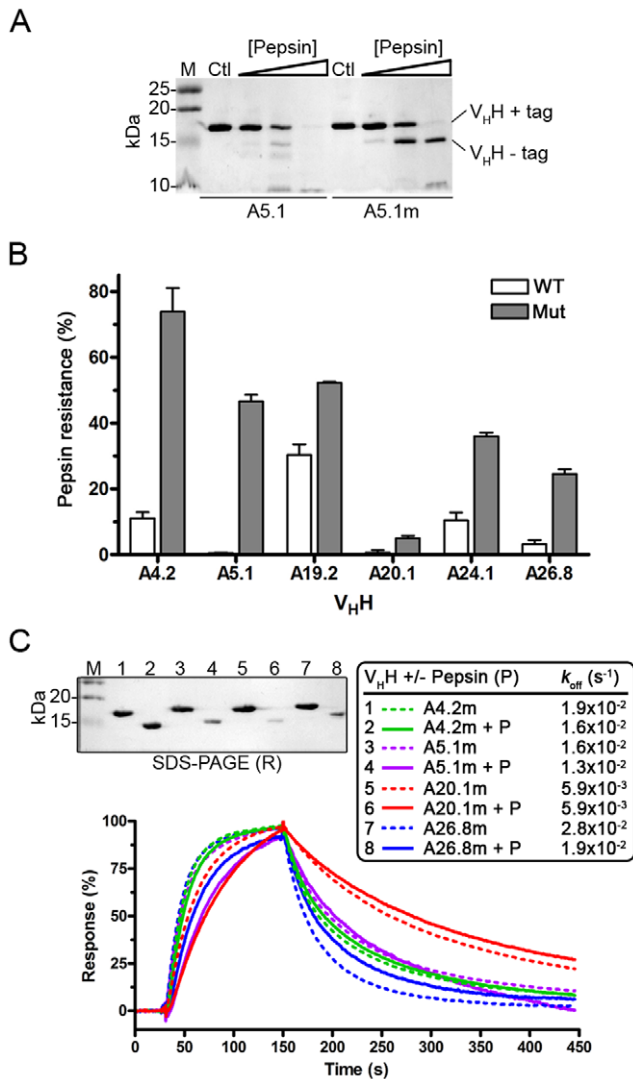

Figure 6. Mutant V_HHs are resistant to pepsin degradation. (**A**) Representative SDS-PAGE analysis showing the separation of A5.1 and A5.1m V_HHs after digestion with various concentrations of pepsin (increasing from left to right: 1 μg/mL, 10 μg/mL and 100 μg/mL) at pH 2.0 and 37°C for 1 h. Control V_HHs (Ctl) were incubated under the same conditions without pepsin. Three micrograms of protein was loaded per lane. Bands appearing ~2 kDa below the full-length V_HH ("V_HH+tag") were identified by MS (data not shown) as V_HHs cleaved within the C-terminal c-Myc tag ("V_HH−tag"), as shown before with protease-digested human V_Hs [61]. (**B**) Summary of V_HH resistance profiles to 100 μg/mL pepsin treatment. Resistance values were obtained by densitometric measurements of pepsin-treated V_HHs relative to controls (as in Fig. 6A). Error bars represent the SEM obtained from 3 independent digestions for each V_HH. (**C**) SPR analysis (*bottom*) on mutant V_HHs digested with pepsin (100 μg/mL, 1 h, 37°C). The pepsin-treated V_HHs retained their ability to bind surface-immobilized TcdA. SDS-PAGE (*top*) showing untreated (lanes 1, 3, 5, 7) and pepsin-digested (lanes 2, 4, 6, 8) V_HHs used for SPR. The contents of lanes 1 thru 8 are described in the box in C. Normalized k_{off}s for pepsin treated V_HHs were similar to the k_{off} of untreated controls (*box* and Table 2). M: molecular weight markers in kDa; WT: wild-type V_HH; Mut: mutant V_HH; P: pepsin; R: reducing SDS-PAGE conditions.
doi:10.1371/journal.pone.0028218.g006

V_HHs were significantly degraded by pepsin. These experiments highlight the profound impact a second disulfide bond in the hydrophobic core has on V_HH conformational stability at low pH and resistance to proteolytic degradation by pepsin.
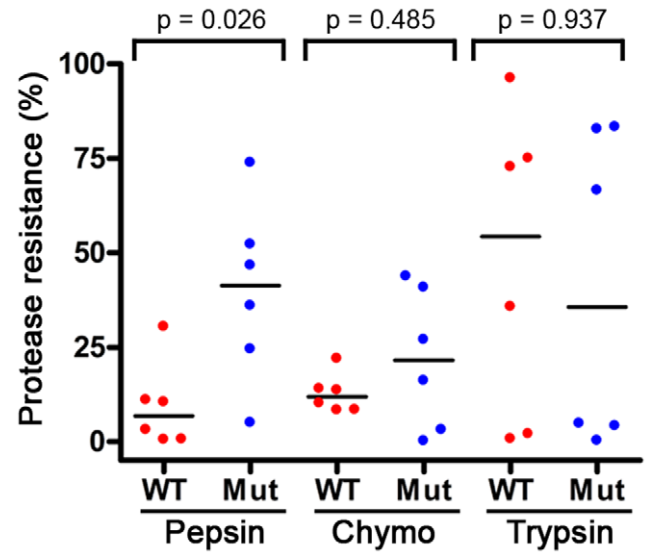
Table 4. Protease resistance profiles of wild-type and mutant V_HHs to the major GI proteases.

V_HH	Pepsin resistance (%)		Chymotrypsin resistance (%)		Trypsin resistance (%)	
	Wild-type	Mutant	Wild-type	Mutant	Wild-type	Mutant
A4.2/A4.2m	11.08±1.88	73.87±7.23	13.60±6.50	3.18±1.10	35.72±7.08	4.80±0.61
A5.1/A5.1m	0.53±0.15	46.63±1.99	14.03±3.15	27.00±4.05	96.23±7.09	83.30±4.96
A19.2/A19.2m	30.37±3.16	52.27±0.32	8.30±1.14	0.18±0.10	0.73±0.73	0.27±0.27
A20.1/A20.1m	0.68±0.68	5.04±0.76	10.17±1.85	16.17±5.26	72.77±4.85	82.80±1.97
A24.1/A24.1m	10.45±2.39	36.02±1.11	22.03±5.01	43.80±2.08	75.03±9.63	66.50±3.58
A26.8/A26.8m	3.17±1.24	24.56±1.45	8.40±1.23	40.83±8.81	2.03±2.03	4.10±1.27

All V_HH digestions were performed at 37°C for 1 h in the presence of 100 µg/mL protease. Resistance values were obtained by comparing the intensity of protease-digested V_HHs relative to untreated controls using SDS-PAGE and imaging software. See Fig. 6A as an example. Values represent the mean ± SEM (n = 3). Data were incorporated into Fig. 6B and Fig. S5.
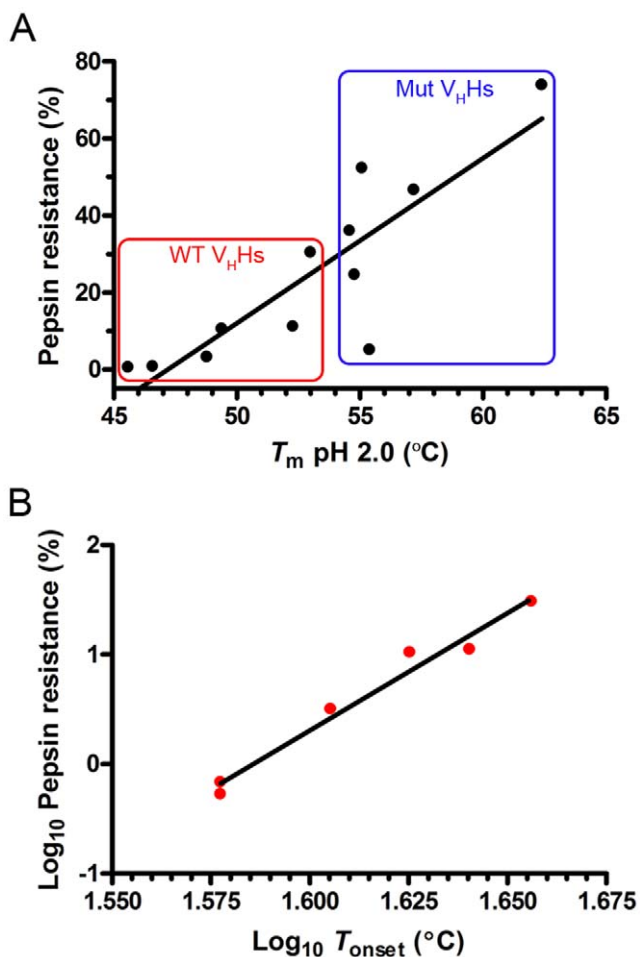doi:10.1371/journal.pone.0028218.t004

Figure 8. Correlation between V_HH pepsin resistance and thermal stability at acidic pH. (**A**) Linear regression between V_HH pepsin resistance and V_HH T_m at pH 2.0. Red and blue boxes show the wild-type (WT) and mutant (Mut) V_HHs, respectively. Linear regression analysis gave a correlation coefficient of $r^2 = 0.735$ and a significantly non-zero slope of the line (p = 0.0004). (**B**) Linear regression between wild-type V_HH pepsin resistance and wild-type V_HH T_{onset} at pH 2.0. The T_{onset} is defined as the temperature at which 5% of the V_HH is unfolded. Linear regression analysis gave a correlation coefficient of $r^2 = 0.975$ and a significantly non-zero slope of the line (p = 0.0002).
doi:10.1371/journal.pone.0028218.g008

To test this hypothesis, we generated the disulfide bond mutants and compared them to their wild-type counterparts containing only the native disulfide bond between residues 23 and 104. Mutant V_HHs were well expressed in *E. coli* when targeted to the periplasmic space, although with lower yields compared to wild-type V_HH counterparts, and all were non-aggregating monomers as determined by size exclusion chromatography. To confirm disulfide bond formation, we used a combination of proteolytic and chemical digestion coupled with MS^2 to precisely identify V_HH peptide fragments harboring the introduced disulfide bond. This approach is preferred over the Ellman's assay approach for the determination of disulfide linkage formation, as it requires less quantities of protein and reveals the positional identity of Cys pairs in a given disulfide bond. The latter information is important, as there is also the possibility that the two engineered Cys residues, besides forming the desired disulfide bond may form undesired disulfide bonds with the two conserved Cys residues at positions 23 and 104. After confirming disulfide bond formation in our mutants, SPR binding experiments revealed most mutant V_HHs possessed 1- to 5-fold weaker affinity constants relative to wild-type, which is consistent with observations by others of up to 3-fold
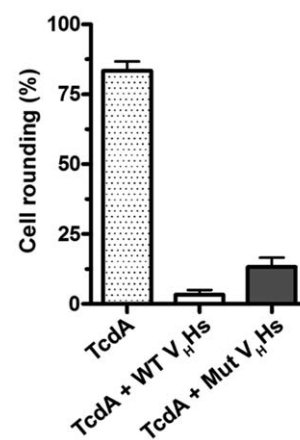

Figure 9. Mutant V_HHs retain TcdA-neutralizing capacity. Confluent monolayers of IMR-90 human lung fibroblasts were incubated with TcdA (100 ng/mL) or TcdA+V_HHs (1000 nM) for 24 h, and the percentage of cells rounded was scored using a light microscope from 0% to 100%. V_HHs (wild-type (WT) or mutant (Mut)) were added as pooled mixtures of A4.2, A5.1, A20.1, and A26.8 (250 nM each) or A4.2m, A5.1m, A20.1m, and A26.8m (250 nM each).
doi:10.1371/journal.pone.0028218.g009

reductions in the affinities of V_HHs containing the same introduced disulfide bond [38,50]. However, for the two weak neutralizing V_HHs, A19.2m and A24.1m, the non-canonical disulfide linkage compromised specificity.

We used CD spectroscopy to compare wild-type and mutant V_HH secondary structure, tertiary structure and thermal stability (T_m and T_{onset}). Comparisons of V_HH secondary and tertiary structure with far-UV and near-UV CD spectroscopy strongly suggested structural differences between wild-type and mutants, at both neutral and acidic pH. For all mutants, peak intensity and selective peak minima shifts were observed, although the overall spectral profiles remained very similar in all wild-type/mutant pairs. More specifically, mutants consistently showed rightward peak shifts in the peak range of 230 nm–235 nm (far-UV CD spectra) and around 297 nm (near-UV CD spectra) compared to wild-type V_HHs. Such patterns may be used as signatures that could be used to quickly identify V_HHs containing a properly formed non-canonical disulfide bond, as could SDS-PAGE motility values since, compared to wild-type V_HHs, mutants consistently moved slower in SDS-PAGE gels. Thus, the far- and near-UV CD spectral data suggests the introduced disulfide bond changes the structure of V_HHs. This is consistent with the observed perturbations in affinities and specificities and increased GI protease resistance of the mutant V_HHs compared to the wild-types (*see below*). We used CD spectroscopy thermal denaturation experiments to show a profound and significant increase in the T_ms and T_{onset}s of mutant V_HHs at both neutral and acidic pH. These mutants are more thermostable than previously reported V_Hs, which were affinity selected from a V_H phage display library under stability pressure [45]. The beneficial effect of the non-canonical disulfide linkage on T_ms varies widely, with T_m increases ranging from $\approx 4°C$ to $\approx 12°C$. This suggests that for the mutant V_HHs with a higher thermostability gain, the non-canonical disulfide linkage may have been a better fit to the overall fold. A19.2m and A24.1m showed the lowest thermostability gains and, if it is true that this is because of an unfit disulfide linkage, it would explain why they were transformed into non-specific binders upon mutation. For A4.2m on the other hand, the non-canonical disulfide linkage seems to be a natural fit, as it increased its T_m the most (by almost $12°C$) and significantly improved GI protease resistance (with the highest increase in pepsin resistance; *see below*), all without adversely affecting the K_D. We also observed a correlation between pepsin resistance and T_m, and this has implications in terms of using heat as the selective pressure for selecting pepsin resistant antibody fragments by *in vitro* evolutionary approaches.

Most likely, mutants (exhibiting higher T_ms) also have higher thermodynamic stability since thermodynamic stability generally increases with T_m [62]. This has been shown to be the case for both V_H and V_HH domains as well [38,45]. In the instance of V_HHs, it has been shown that the introduction of the Cys54/Cys78 disulfide linkage used in our study into V_HHs led to increases in both T_m and thermodynamic stability. Proteins with higher T_m are also less likely to unfold [62]. These may be the reasons why our mutants were more resistant to acid-induced unfolding at $37°C$, supported by the higher T_{onset}s and pepsin resistance of our mutant V_HHs (*see below*). Consistent with this, in a previous study, human V_Hs which were more resistant to acid-induced aggregation, a phenomenon encouraged/initiated by protein unfolding, had higher T_ms and thermodynamic stabilities [45]. The improved reversibility of thermal unfolding of mutant V_HHs compared to their wild-type counterparts under acidic conditions in our work (data not shown) indicates that the introduced disulfide linkage may also render V_HHs with

aggregation resistant unfolded states [48], in addition to higher thermodynamic stability. Hagihara et al [37] showed that the introduction of the same Cys54/Cys78 disulfide linkage into a V_HH, in addition to increasing its T_m, led to decreases in its enthalpy and entropy changes of unfolding. The enthalpy and entropy measurements indicated that the stabilization effect of the extra disulfide linkage in V_HHs may be related to factors such as loop entropy, internal interactions such as hydrogen bonding and van der Waals interactions and hydration of the native and unfolded states.

We also examined the resistance profiles of the disulfide bond mutants to the major GI proteases. Mutant V_HHs were universally more resistant to pepsin and many were more resistance to chymotrypsin when compared to their wild-type counterparts. Protease sensitivity is a function of many variables including the location of proteolytic sites (e.g., loops *vs* protein core in antibodies), the theoretical number of proteolytic sites, and protein compactness and thermodynamic stability [63,64]. Since each wild-type and mutant V_HH pair possessed the identical number of theoretical protease cleavage sites, we speculate that the second disulfide bond presents a more compact and thermodynamically stable V_HH structure, preventing pepsin and chymotrypsin from accessing proteolytic cleavage sites. This view is consistent with the increased T_ms in mutants (an indicator of mutants' increased thermostability), the positive correlation between pepsin resistance and T_m (Fig. 8), and the lack of correlation between pepsin/chymotrypsin resistance and the number of theoretical protease cleavage sites (Fig. S6). The pepsin resistance *vs* T_m/T_{onset} correlation curves also point to the fact that structural compactness and thermodynamic stability plays a more prominent role in pepsin resistance, which is understandable given that pepsin requires protein unfolding for efficient digestion. This benefit is not realized for mutants against trypsin, possibly because their cleavage sites are at hydrophilic residues (Lys or Arg) which must be in more exposed regions of the V_HH, possibly located in the CDR regions. Further, these regions would not be protected by stabilizing the core of the structure. The positive correlation between V_HH trypsin resistance and the number of theoretical trypsin cleavage sites is a testament to this (Fig. S6). Harmsen et al [49] have suggested the CDR regions of V_HHs to be the most sensitive sites to proteolysis due to their flexibility and exposed position relative to the V_HH core. Indeed, there are more predicted trypsin-cleavage sites in the CDR regions (Table S3; Fig. S6) of trypsin-sensitive V_HHs (A4.2, A19.2 and A26.8) compared to trypsin-resistant V_HHs (A5.1, A20.1 and A24.1). This is not the case for pepsin and chymotrypsin sensitivities (Table S3; Fig. S6).

Importantly, we also observed an increase in T_{onset} temperatures for mutants at the physiological conditions representative of the stomach (pH $\cong$ 2.0 and $37°C$) to values significantly above $37°C$ (T_{onset}s from $45°C–53°C$). This suggests that the mutants should remain fully folded at $37°C$ in the stomach, hence resisting pepsin degradation (and denaturation) to a higher extent than wild-type V_HHs, a statement supported by our *in vitro* pepsin digestion experiments. In contrast to the mutants, 3 wild-type V_HHs, for example, have low T_{onset} values of $37.8°C$ (A5.1 and A20.1) and $40.3°C$ (A26.8) which suggests they would partially unfold in the stomach (pH $\cong$ 2.0, $37°C$), increasing their proteolytic susceptibility. This indeed is the case in an *in vitro* setting as A5.1 and A20.1, V_HHs with T_{onset} temperatures overlapping the physiological temperature, are completely pepsin sensitive, and A26.8 with a T_{onset} slightly above the physiological temperature, although somewhat better than the former two, is barely resistant to pepsin (pepsin resistance: $\approx 3\%$). In the corresponding pepsin resistant mutants, acquiring resistance

parallels an increase in T_{onset}. In line with these findings, we observe a strong positive correlation between pepsin resistance and T_{onset} (Fig. 8), and depending on the melting curve profile, T_{onset}s may be better predictors of protein pepsin resistance than T_ms.

Compared to other studies involving *in vitro* V_HH proteolysis, our mutant V_HHs performed remarkably well, withstanding near physiological concentrations of pepsin and chymotrypsin and retaining functionality thereafter. Additionally, half of the mutants were trypsin resistant and for those which were not, identification and removal of their cleavage site(s) should be straightforward, e.g., by MS analysis and site-directed mutagenesis. Balan et al [65] note the human stomach contains pepsin concentrations ranging from 500 µg/mL to 1 mg/mL, while Schmidt et al [66] found the average pepsin concentration in the stomach of piglets to be 155 U/mL. Our pepsin digestion assays were performed at 100 µg/mL concentrations, which correspond to 46 U/mL. The most stable V_HH mutant produced by Harmsen et al [49] using a DNA shuffling approach showed only 21% residual V_HH remaining after digestion with 100 µg/mL of pepsin. In contrast, our most stable V_HH (A4.2m) showed 74% residual V_HH remaining after digestion, while 4 others had residual pepsin resistance values of 24% or higher. In addition, all 4 disulfide bond mutant V_HHs retained binding to TcdA after pepsin treatment, confirming their resistance to the protease and retention of functionality.

We also examined the toxin A neutralizing efficacy of our disulfide bond mutant V_HHs. Compared to the wild-type V_HHs, the mutants were 3–4 fold weaker with respect to toxin A neutralization in cell-based assays, presumably a reflection in the reduced affinities of 3 of 4 V_HHs for the toxin. If a more thorough analysis was performed on individual V_HHs, it is possible that clone A4.2m, which showed the same affinity as A4.2 for toxin A, might be a more potent neutralizer due to its higher stability. Under stringent conditions *in vivo*, the lower affinity mutants may actually be more efficacious than the higher affinity wild-type V_HHs due to their greater stability, as shown elsewhere [50]. Also, a number of methods are available to increase the affinity of the disulfide-stabilized domains, allowing for the creation of superpotent toxin A neutralizing antibodies capable of withstanding a wide range of harsh conditions.

In conclusion, we have shown that the introduction of a second disulfide bond into the hydrophobic core of a panel of llama V_HHs increased thermal stability and GI protease resistance; the approach is both effective and general. The approach does not come without some drawbacks, including, reduced affinity, specificity, and expression yield. However, the mutants outperformed the wild-type V_HHs under more stringent physiological conditions, which outweighs the reductions in affinity, as noted above. Whether the mutant V_HHs are more efficacious than the wild-type V_HHs *in vivo* remains to be determined. Based on our results and those of others, we suggest incorporating the non-canonical disulfide bond between position 54 and 78 at the library construction phase and not after the selection/screening phase to avoid adverse side effects on affinity and specificity seen here and in other studies. Other approaches, such as affinity maturation, could be used to overcome losses in target affinity as a result of disulfide bond incorporation. Our mutant V_HHs are ideal building blocks for oral therapeutic agents that must survive the harsh GI tract, and provide promising alternatives to antibiotics. The oral administration of therapeutic proteins is of interest to the pharmaceutical and biotechnological industries [29,63,67,68]. Protein-based oral therapeutics have several conceived advantages over systemic administration: convenience, patience compliance, lower cost, pain-free administration, drug purity, flexibility in production source (i.e., bacterial, plant, etc.), and fewer concerns over immunogenicity. Despite the many advantages of orally administering protein therapeutics, few successes have been realized due to the destabilizing environment of the GI tract. Of the major GI proteases, pepsin is considered the primary cause of antibody degradation [29,35,49] and hence a major obstacle facing orally delivered antibody therapeutics. Regarding the mutant V_HHs generated in this study, the therapeutic efficacy can be further enhanced by improving their affinity (through selection of affinity maturation display libraries) and by formulation. The affinity maturation libraries could yield V_HHs which are hyper-stabilized (e.g., high GI protease resistance) in addition to being of ultra-high affinity, if selection pressures (acid, proteases, heat) are applied during the panning stage [43,45]. Indeed, the correlation between V_HH pepsin resistance and T_m suggests that selection under heat should produce pepsin-resistant V_HHs. Given their stability profile, the mutants may be resistant to serum degradation, making them efficacious systemic therapeutics if they are coupled to a half-life extending molecule. Other applications for our stabilized domains include: (i) use as delivery agents for mucosal vaccines [69] or (ii) use as robust affinity purification reagents resistant to acidic and heat elution steps. Furthermore, the recent incorporation of these engineered disulfide bonds into human V_H sdAbs not only resulted in increased thermal stability, but also markedly reduced V_H aggregation [70], suggesting that the introduced disulfide bond imparts a universal stabilizing effect in all immunoglobulin variable domains.

Supporting Information

Figure S1 Alignment and comparison of wild-type and mutant V_HH amino acid sequences. Wild-type V_HH sequences are shown with a single disulfide bond between Cys^{23} and Cys^{104}. A second disulfide bond was introduced through mutation of Ala^{54}/Gly^{54} and Ile^{78} to Cys^{54} (*) and Cys^{78} in framework region 2 (FR2) and FR3, respectively. Disulfide bonds are shown as black lines. Residues colored in blue illustrate the disulfide bond-linked peptides identified by nanoRPLC-ESI-MS analysis on CNBr and trypsin digested mutant V_HHs (Fig. 2). Amino acid numbering and CDR designation is based on the IMGT system (http://imgt.cines.fr/).
(TIF)

Figure S2 Far-UV CD analysis of V_HHs at neutral and acidic pH. CD scans (210 nm–260 nm) were performed at 25°C on V_HHs (50 µg/mL) equilibrated for 2 h in 10 mM sodium phosphate buffer (pH 7.3) or 10 mM sodium phosphate buffer+50 mM HCl (pH 2.0). The spectra represent the mean residue ellipticity of 8 data accumulations collected from 2 independent experiments. Raw data were smoothed using the Jasco software and converted to mean residue ellipticity as described in *Methods*. Red lines: wild-type V_HH at pH 7.3; blue lines: mutant V_HH at pH 7.3; green lines: wild-type V_HH at pH 2.0; orange lines: mutant V_HH at pH 2.0.
(TIF)

Figure S3 Near-UV CD analysis of V_HHs at neutral and acidic pH. CD scans (250 nm–340 nm) were performed at 25°C on V_HHs (250 µg/mL) equilibrated for 2 h in 10 mM sodium phosphate buffer (pH 7.3) or 10 mM sodium phosphate buffer+50 mM HCl (pH 2.0). The spectra represent the mean residue ellipticity from 8 data accumulations collected from 2 independent experiments. Raw data were smoothed using the Jasco software and converted to mean residue ellipticity as described in *Methods*. Red lines: wild-type V_HH at pH 7.3; blue lines: mutant V_HH at

pH 7.3; green lines: wild-type V$_H$H at pH 2.0; orange lines: mutant V$_H$H at pH 2.0.
(TIF)

Figure S4 V$_H$H thermal unfolding curves. (A) Thermal unfolding of wild-type and mutant V$_H$Hs (50 µg/mL) at pH 7.3 (10 mM sodium phosphate buffer) and pH 2.0 (10 mM sodium phosphate buffer+50 mM HCl) were followed at 215 nm to identify the thermal unfolding midpoint temperature (T_m). The T_m was determined for each curve by Boltzmann non-linear curve fitting analysis in GraphPad Prism. The goodness of curve fit (r^2) ranged from 0.9901–0.9995. In the case of V$_H$Hs with few lower baseline data points the T_m is a minimal estimate (see Table 3). Red lines: wild-type V$_H$H at pH 7.3; blue lines: mutant V$_H$H at pH 7.3; green lines: wild-type V$_H$H at pH 2.0; orange lines: mutant V$_H$H at pH 2.0. **(B)** Raw thermal unfolding data used to generate the normalized curves in (A).
(TIF)

Figure S5 V$_H$H resistance profiles against trypsin and chymotrypsin. Wild-type (WT) and mutant (Mut) V$_H$Hs were digested with 100 µg/mL of chymotrypsin or trypsin for 1 h at 37°C and separated by SDS-PAGE. Resistance values were calculated as in Fig. 6.
(TIF)

Figure S6 Correlation between V$_H$H protease resistance and the number of theoretical proteolytic cleavage sites. Linear regression between V$_H$H protease resistance and the number of theoretical cleavage sites within the whole V$_H$H ("Total sites") or within the IMGT-defined CDR regions ("CDR sites"). Wild-type and mutant V$_H$H protease resistance values were combined for each protease. The number of protease cleavage sites was determined as in Table S3. Linear regression analysis was used to analyze the correlation coefficient (r^2) and significantly non-zero slope of the line (p) in each graph.
(TIF)

Table S1 Primers used in this study.
(PDF)

Table S2 Onset temperatures (T_{onset}s) of wild-type and mutant V$_H$Hs.
(PDF)

Table S3 Theoretical number of protease cleavable sites located within V$_H$Hs.
(PDF)

Acknowledgments

Author Contributions

Conceived and designed the experiments: GH RM JT. Performed the experiments: GH TH WD. Analyzed the data: GH TH WD RM JT. Wrote the paper: GH JT.

References

1. Cegelski L, Marshall GR, Eldridge GR, Hultgren SJ (2008) The biology and future prospects of antivirulence therapies. Nat Rev Microbiol 6: 17–27.
2. Clatworthy AE, Pierson E, Hung DT (2007) Targeting virulence: a new paradigm for antimicrobial therapy. Nat Chem Biol 3: 541–548.
3. Lynch SV, Wiener-Kronish JP (2008) Novel strategies to combat bacterial virulence. Curr Opin Crit Care 14: 593–599.
4. Svensson A, Larsson A, Emtenäs H, Hedenström M, Fex T, et al. (2001) Design and evaluation of pilicides: potential novel antibacterial agents directed against uropathogenic Escherichia coli. Chembiochem 2: 915–918.
5. Panchal RG, Hermone AR, Nguyen TL, Wong TY, Schwarzenbacher R, et al. (2004) Identification of small molecule inhibitors of anthrax lethal factor. Nat Struct Mol Biol 11: 67–72.
6. Shoop WL, Xiong Y, Wiltsie J, Woods A, Guo J, et al. (2005) Anthrax lethal factor inhibition. Proc Natl Acad Sci U S A 102: 7958–7963.
7. Muschiol S, Bailey L, Gylfe A, Sundin C, Hultenby K, et al. (2006) A small-molecule inhibitor of type III secretion inhibits different stages of the infectious cycle of Chlamydia trachomatis. Proc Natl Acad Sci U S A 103: 14566–14571.
8. Hudson DL, Layton AN, Field TR, Bowen AJ, Wolf-Watz H, et al. (2007) Inhibition of type III secretion in Salmonella enterica serovar Typhimurium by small-molecule inhibitors. Antimicrob Agents Chemother 51: 2631–2635.
9. Lyon GJ, Wright JS, Muir TW, Novick RP (2002) Key determinants of receptor activation in the agr autoinducing peptides of Staphylococcus aureus. Biochemistry 41: 10095–10104.
10. Thiagarajah JR, Verkman AS (2005) New drug targets for cholera therapy. Trends Pharmacol Sci 26: 172–175.
11. Kurtz CB, Cannon EP, Brezzani A, Pitruzzello M, Dinardo C, et al. (2001) GT160-246, a toxin binding polymer for treatment of Clostridium difficile colitis. Antimicrob Agents Chemother 45: 2340–2347.
12. Hinkson PL, Dinardo C, DeCiero D, Klinger JD, Barker RH, Jr. (2008) Tolevamer, an anionic polymer, neutralizes toxins produced by the BI/027 strains of Clostridium difficile. Antimicrob Agents Chemother 52: 2190–2195.
13. Schneemann A, Manchester M (2009) Anti-toxin antibodies in prophylaxis and treatment of inhalation anthrax. Future Microbiol 4: 35–43.
14. Strockbine NA, Marques LR, Holmes RK, O'Brien AD (1985) Characterization of monoclonal antibodies against Shiga-like toxin from Escherichia coli. Infect Immun 50: 695–700.
15. Peterson JW, Hejtmancik KE, Markel DE, Craig JP, Kurosky A (1979) Antigenic specificity of neutralizing antibody to cholera toxin. Infect Immun 24: 774–779.
16. Nowakowski A, Wang C, Powers DB, Amersdorfer P, Smith TJ, et al. (2002) Potent neutralization of botulinum neurotoxin by recombinant oligoclonal antibody. Proc Natl Acad Sci U S A 99: 11346–11350.
17. LowyI, Molrine DC, Leav BA, Blair BM, Baxter R, et al. (2010) Treatment with monoclonal antibodies against Clostridium difficile toxins. N Engl J Med 362: 197–205.
18. Kink JA, Williams JA (1998) Antibodies to recombinant Clostridium difficile toxins A and B are an effective treatment and prevent relapse of C. difficile-associated disease in a hamster model of infection. Infect Immun 66: 2018–2025.
19. Babcock GJ, Broering TJ, Hernandez HJ, Mandell RB, Donahue K, et al. (2006) Human monoclonal antibodies directed against toxins A and B prevent Clostridium difficile-induced mortality in hamsters. Infect Immun 74: 6339–6347.
20. Hussack G, Arbabi-Ghahroudi M, van Faassen H, Songer JG, Ng KK, et al. (2011) Neutralization of Clostridium difficile toxin A with single-domain antibodies targeting the cell receptor binding domain. J Biol Chem 286: 8961–8976.
21. Hussack G, Tanha J (2010) Toxin-specific antibodies for the treatment of Clostridium difficile: current status and future perspectives. Toxins 2: 998–1018.
22. Bebbington C, Yarranton G (2008) Antibodies for the treatment of bacterial infections: current experience and future prospects. Curr Opin Biotechnol 19: 613–619.
23. Jank T, Aktories K (2008) Structure and mode of action of clostridial glucosylating toxins: the ABCD model. Trends Microbiol 16: 222–229.
24. Tjellström B, Stenhammar L, Eriksson S, Magnusson KE (1993) Oral immunoglobulin A supplement in treatment of Clostridium difficile enteritis. Lancet 341: 701–702.
25. Davidson GP, Whyte PB, Daniels E, Franklin K, Nunan H, et al. (1989) Passive immunisation of children with bovine colostrum containing antibodies to human rotavirus. Lancet 2: 709–712.
26. Tacket CO, Binion SB, Bostwick E, Losonsky G, Roy MJ, et al. (1992) Efficacy of bovine milk immunoglobulin concentrate in preventing illness after Shigella flexneri challenge. Am J Trop Med Hyg 47: 276–283.
27. Tacket CO, Losonsky G, Link H, Hoang Y, Guesry P, et al. (1988) Protection by milk immunoglobulin concentrate against oral challenge with enterotoxigenic Escherichia coli. N Engl J Med 318: 1240–1243.
28. Yokoyama H, Peralta RC, Diaz R, Sendo S, Ikemori Y, et al. (1992) Passive protective effect of chicken egg yolk immunoglobulins against experimental enterotoxigenic Escherichia coli infection in neonatal piglets. Infect Immun 60: 998–1007.
29. Reilly RM, Domingo R, Sandhu J (1997) Oral delivery of antibodies. Future pharmacokinetic trends. Clin Pharmacokinet 32: 313–323.
30. Hamers-Casterman C, Atarhouch T, Muyldermans S, Robinson G, Hamers C, et al. (1993) Naturally occurring antibodies devoid of light chains. Nature 363: 446–448.
31. Arbabi Ghahroudi M, Desmyter A, Wyns L, Hamers R, Muyldermans S (1997) Selection and identification of single domain antibody fragments from camel heavy-chain antibodies. FEBS Lett 414: 521–526.

32. Wesolowski J, Alzogaray V, Reyelt J, Unger M, Juarez K, et al. (2009) Single domain antibodies: promising experimental and therapeutic tools in infection and immunity. Med Microbiol Immunol 198: 157–174.

33. Harmsen MM, van Solt CB, Hoogendoorn A, van Zijderveld FG, Niewold TA, et al. (2005) *Escherichia coli* F4 fimbriae specific llama single-domain antibody fragments effectively inhibit bacterial adhesion *in vitro* but poorly protect against diarrhoea. Vet Microbiol 111: 89–98.

34. Krüger C, Hultberg A, Marcotte H, Hermans P, Bezemer S, et al. (2006) Therapeutic effect of llama derived VHH fragments against *Streptococcus mutans* on the development of dental caries. Appl Microbiol Biotechnol 72: 732–737.

35. van der Vaart JM, Pant N, Wolvers D, Bezemer S, Hermans PW, et al. (2006) Reduction in morbidity of rotavirus induced diarrhoea in mice by yeast produced monovalent llama-derived antibody fragments. Vaccine 24: 4130–4137.

36. Young NM, MacKenzie CR, Narang SA, Oomen RP, Baenziger JE (1995) Thermal stabilization of a single-chain Fv antibody fragment by introduction of a disulphide bond. FEBS Lett 377: 135–139.

37. Hagihara Y, Mine S, Uegaki K (2007) Stabilization of an immunoglobulin fold domain by an engineered disulfide bond at the buried hydrophobic region. J Biol Chem 282: 36489–36495.

38. Saerens D, Conrath K, Govaert J, Muyldermans S (2008) Disulfide bond introduction for general stabilization of immunoglobulin heavy-chain variable domains. J Mol Biol 377: 478–488.

39. Gong R, Vu BK, Feng Y, Prieto DA, Dyba MA, et al. (2009) Engineered human antibody constant domains with increased stability. J Biol Chem 284: 14203–14210.

40. Wörn A, Plückthun A (1998) Mutual stabilization of V_L and V_H in single-chain antibody fragments, investigated with mutants engineered for stability. Biochemistry 37: 13120–13127.

41. Sieber V, Plückthun A, Schmid FX (1998) Selecting proteins with improved stability by a phage-based method. Nat Biotechnol 16: 955–960.

42. Jung S, Honegger A, Plückthun A (1999) Selection for improved protein stability by phage display. J Mol Biol 294: 163–180.

43. Jermutus L, Honegger A, Schwesinger F, Hanes J, Plückthun A (2001) Tailoring *in vitro* evolution for protein affinity or stability. Proc Natl Acad Sci U S A 98: 75–80.

44. Matsuura T, Plückthun A (2003) Selection based on the folding properties of proteins with ribosome display. FEBS Lett 539: 24–28.

45. Famm K, Hansen L, Christ D, Winter G (2008) Thermodynamically stable aggregation-resistant antibody domains through directed evolution. J Mol Biol 376: 926–931.

46. Famm K, Winter G (2006) Engineering aggregation-resistant proteins by directed evolution. Protein Eng Des Sel 19: 479–481.

47. Christ D, Famm K, Winter G (2007) Repertoires of aggregation-resistant human antibody domains. Protein Eng Des Sel 20: 413–416.

48. Jespers L, Schon O, Famm K, Winter G (2004) Aggregation-resistant domain antibodies selected on phage by heat denaturation. Nat Biotechnol 22: 1161–1165.

49. Harmsen MM, van Solt CB, van Zijderveld-van Bemmel AM, Niewold TA, van Zijderveld FG (2006) Selection and optimization of proteolytically stable llama single-domain antibody fragments for oral immunotherapy. Appl Microbiol Biotechnol 72: 544–551.

50. Chan PH, Pardon E, Menzer L, De Genst E, Kumita JR, et al. (2008) Engineering a camelid antibody fragment that binds to the active site of human lysozyme and inhibits its conversion into amyloid fibrils. Biochemistry 47: 11041–11054.

51. Arbabi-Ghahroudi M, MacKenzie R, Tanha J (2009) Selection of non-aggregating V_H binders from synthetic V_H phage-display libraries. Methods Mol Biol 525: 187–216, xiii.

52. Ho SN, Hunt HD, Horton RM, Pullen JK, Pease LR (1989) Site-directed mutagenesis by overlap extension using the polymerase chain reaction. Gene 77: 51–59.

53. Arbabi-Ghahroudi M, Mackenzie R, Tanha J (2010) Site-directed mutagenesis for improving biophysical properties of V_H domains. Methods Mol Biol 634: 309–330.

54. Greenfield NJ (2006) Using circular dichroism spectra to estimate protein secondary structure. Nat Protoc 1: 2876–2890.

55. Greenfield NJ (2006) Analysis of the kinetics of folding of proteins and peptides using circular dichroism. Nat Protoc 1: 2891–2899.

56. Bordoli L, Kiefer F, Arnold K, Benkert P, Battey J, et al. (2009) Protein structure homology modeling using SWISS-MODEL workspace. Nat Protoc 4: 1–13.

57. Spinelli S, Frenken LG, Hermans P, Verrips T, Brown K, et al. (2000) Camelid heavy-chain variable domains provide efficient combining sites to haptens. Biochemistry 39: 1217–1222.

58. Saerens D, Kinne J, Bosmans E, Wernery U, Muyldermans S, et al. (2004) Single domain antibodies derived from dromedary lymph node and peripheral blood lymphocytes sensing conformational variants of prostate-specific antigen. J Biol Chem 279: 51965–51972.

59. Wu SL, Jiang H, Lu Q, Dai S, Hancock WS, et al. (2009) Mass spectrometric determination of disulfide linkages in recombinant therapeutic proteins using online LC-MS with electron-transfer dissociation. Anal Chem 81: 112–122.

60. Dumoulin M, Conrath K, Van Meirhaeghe A, Meersman F, Heremans K, et al. (2002) Single-domain antibody fragments with high conformational stability. Protein Sci 11: 500–515.

61. To R, Hirama T, Arbabi-Ghahroudi M, MacKenzie R, Wang P, et al. (2005) Isolation of monomeric human V_Hs by a phage selection. J Biol Chem 280: 41395–41403.

62. Wang W, Nema S, Teagarden D (2010) Protein aggregation–pathways and influencing factors. Int J Pharm 390: 89–99.

63. Hubbard SJ, Beynon RJ, Thornton JM (1998) Assessment of conformational parameters as predictors of limited proteolytic sites in native protein structures. Protein Eng 11: 349–359.

64. Frenken LG, Egmond MR, Batenburg AM, Verrips CT (1993) *Pseudomonas glumae* lipase: increased proteolytic stability by protein engineering. Protein Eng 6: 637–642.

65. Balan KK, Jones AT, Roberts NB, Pearson JP, Critchley M, et al. (1996) The effects of *Helicobacter pylori* colonization on gastric function and the incidence of portal hypertensive gastropathy in patients with cirrhosis of the liver. Am J Gastroenterol 91: 1400–1406.

66. Schmidt P, Wiedemann V, Kühlmann R, Wanke R, Linckh E, et al. (1989) Chicken egg antibodies for prophylaxis and therapy of infectious intestinal diseases. II. *In vitro* studies on gastric and enteric digestion of egg yolk antibodies specific against pathogenic *Escherichia coli* strains. Zentralbl Veterinarmed B 36: 619–628.

67. Amorij JP, Hinrichs W, Frijlink HW, Wilschut JC, Huckriede A (2010) Needle-free influenza vaccination. Lancet Infect Dis 10: 699–711.

68. Werle M, Makhlof A, Takeuchi H (2009) Oral protein delivery: a patent review of academic and industrial approaches. Recent Pat Drug Deliv Formul 3: 94–104.

69. Li S, Zheng W, Kuolee R, Hirama T, Henry M, et al. (2009) Pentabody-mediated antigen delivery induces antigen-specific mucosal immune response. Mol Immunol 46: 1718–1726.

70. Kim DY, Ding W, Tanha J (2011) Solubility and stability engineering of human V_H domains. Methods Mol Biol;(In press).